

# Scaling Wideband Massive MIMO Radar via Tiled Beamspace Processing

Oveys Delafrooz Noroozi\*, Jiyeon Han<sup>†</sup>, Wei Tang<sup>†</sup>, Zhengya Zhang<sup>†</sup>,  
Upamanyu Madhow\*

\*University of California, Santa Barbara, CA, U.S.A., <sup>†</sup>University of Michigan, Ann Arbor, MI, U.S.A.  
{oveys, madhow}@ucsb.edu {hanjyeon, weitang, zhengya}@umich.edu

**Abstract**—We present a coordinated tiled architecture for scalable wideband digital beamforming in massive MIMO radar systems. As aperture size increases, conventional full-array MVDR processing becomes prohibitive due to the cubic complexity of covariance estimation and inversion. Building on the principle of energy concentration in beamspace, we introduce a tiled windowed-beamspace MVDR framework that distributes spatial FFT processing across subarrays while performing joint beamforming in a compact global beamspace domain. Each tile applies a 2D spatial DFT followed by an angle-of-arrival dependent beamspace window, producing a reduced-dimensional representation that preserves the dominant spatial structure of the received signal. The windowed outputs from the tiles are concatenated and processed by a centralized MVDR beamformer, enabling coherent full-aperture processing with drastically reduced dimensionality. Our numerical results demonstrate that the proposed architecture achieves detection and interference suppression performance comparable to full-dimensional processing, while substantially lowering computational cost, memory usage, and training requirements. The framework also reveals tradeoffs among tile size, window size, and beamspace resolution that govern overall system scalability.

**Index Terms**—Beamspace processing, tiled arrays, MVDR beamforming, massive MIMO radar, target detection

## I. INTRODUCTION

Fully digital wideband MIMO radar arrays offer the ability to form multiple beams simultaneously for target detection, tracking, and interference suppression, in contrast to the sequential scanning beams of traditional phased arrays. Continued advances in RF integration and digital processing are rapidly making massive digital arrays—featuring hundreds or thousands of elements—feasible for next-generation radar systems. However, the computational burden associated with conventional spatial processing presents a fundamental obstacle to such scaling. Classical minimum variance distortionless response (MVDR) beamforming requires the estimation and inversion of an  $N \times N$  sample covariance matrix, leading to  $O(N^3)$  complexity, which becomes prohibitive for large-aperture arrays.

Beamspace processing provides a promising pathway to overcoming this limitation. For regularly spaced arrays, the spatial signature of a plane wave is a complex exponential, enabling its energy to be concentrated by a spatial FFT. Beamspace ideas have long been explored to improve robustness and reduce computational load across a broad range of radar and array-processing applications, including through-

the-wall radar imaging [1], [2], weather radar [3], moving-target localization [4], [5], and subarray-based interference mitigation [6]. Early work on partial adaptation and beamspace MUSIC also demonstrated the benefits of dimension reduction for high-resolution applications [7]. More recently, beamspace dimension-reduction strategies have been successfully employed in multiuser MIMO communication, where user energy often concentrates within a small beamspace region [8], [9], with validation via channel models derived from measured data presented in [10]. These developments motivate the use of beamspace techniques as an enabling mechanism for scalable adaptive all-digital processing in massive arrays for radar.

Our earlier work [11] demonstrated that energy concentration in beamspace enables wideband windowed-beamspace MVDR processing with complexity scaling dominated by the  $O(N \log N)$  cost of spatial FFTs. However, even with beamspace dimension reduction, further architectural innovations are required to support *spatially massive* arrays whose total aperture exceeds what can be processed as a single monolithic block. Recent tiled array architectures—proposed for massive phased arrays and hybrid processing in communication systems [12] partition the array into smaller subarrays (“tiles”) for scalability, but require careful coordination to achieve coherent full-aperture performance.

In this paper, we extend beamspace-MVDR radar processing to a *coordinated tiled* architecture designed for massive wideband arrays. Each tile performs a local 2D spatial FFT followed by an angle-of-arrival dependent beamspace window that extracts only the dominant DFT bins for a given target direction. The windowed outputs from all tiles are then concatenated and processed jointly in a low-dimensional global beamspace domain using MVDR beamforming. This approach distributes the computationally heavy spatial transforms across tiles while keeping covariance estimation and beamforming centralized but low-dimensional. As a result, the system achieves coherent full-aperture performance with drastically reduced computational and memory requirements.

## II. SYSTEM MODEL

### A. Received Signal Model

We consider a two-dimensional uniform planar array (UPA) partitioned into  $T_z \times T_x$  tiles, resulting in a total of  $T = T_z T_x$  tiles. Each tile consists of  $N_z$  vertical and  $N_x$  horizontal antenna elements, for a total of  $N = N_z N_x$  antennas per tile. All

tiles share a common transmit waveform and are synchronized in both time and frequency. The array elements are uniformly spaced with inter-element spacing  $d = \lambda/2$ , where  $\lambda$  is the wavelength corresponding to the design frequency  $f_d$ .

The azimuth and elevation angles of a  $k$ -th received signal are denoted by  $(\varphi_k, \theta_k)$ . The corresponding reference spatial frequencies at the design frequency  $f_d$  are

$$\mathbf{\Omega}_k^{\text{ref}} = \pi \begin{bmatrix} \cos \theta_k \sin \varphi_k \\ \sin \theta_k \end{bmatrix}. \quad (1)$$

At any processing frequency  $f$ , the spatial frequencies scale linearly as

$$\mathbf{\Omega}_k(f) = \begin{bmatrix} \Omega_{k,x}(f) \\ \Omega_{k,z}(f) \end{bmatrix} = \frac{f}{f_d} \mathbf{\Omega}_k^{\text{ref}}. \quad (2)$$

For a uniform linear array of  $N$  elements and spatial frequency  $\Omega$ , the steering vector is defined as

$$\mathbf{u}_N(\Omega) = [1 \quad e^{j\Omega} \quad \dots \quad e^{j(N-1)\Omega}]^T. \quad (3)$$

Accordingly,  $\boldsymbol{\psi}_k(f) \in \mathbb{C}^N$  is the in-tile (element-level) array response for the  $k$ -th source

$$\boldsymbol{\psi}_k(f) = \mathbf{u}_{N_x}(\Omega_{k,x}(f)) \otimes \mathbf{u}_{N_z}(\Omega_{k,z}(f)), \quad (4)$$

The tile-level array response is defined using the same construction applied to the tile grid:

$$\boldsymbol{\Psi}_k(f) = \mathbf{u}_{T_x}(N_x \Omega_{k,x}(f)) \otimes \mathbf{u}_{T_z}(N_z \Omega_{k,z}(f)), \quad (5)$$

where  $\boldsymbol{\Psi}_k(f) \in \mathbb{C}^T$  describes the spatial phase progression across tiles.

The per-tile steering vector observed by tile  $t$  is therefore expressed as

$$\mathbf{a}_k^{(t)}(f) = [\boldsymbol{\Psi}_k(f)]_t \boldsymbol{\psi}_k(f), \quad t = 1, \dots, T. \quad (6)$$

The received snapshot at a given subband and tile  $t$  is modeled as

$$\mathbf{y}^{(t)}[n] = \sum_{k=1}^K \alpha_k^{(t)} \mathbf{a}_k^{(t)} p_k[n - \tau_k] + \mathbf{I}^{(t)}[n] + \mathbf{n}^{(t)}[n], \quad (7)$$

where

- $\alpha_k^{(t)} \in \mathbb{C}$  is the complex gain of the  $k$ -th source,
- $p_k[\cdot]$  is the transmit pulse delayed by  $\tau_k$ ,
- $\mathbf{I}^{(t)}[n]$  models interference or clutter at tile  $t$ ,
- $\mathbf{n}^{(t)}[n] \sim \mathcal{CN}(\mathbf{0}, \sigma_t^2 \mathbf{I})$  denotes spatially white noise.

The frequency (subband) index is omitted for notational simplicity, as the signal model is identical across all subbands.

To simplify notation when combining tile-level quantities, we introduce the concatenation operator

$$\left\{ \mathbf{x}^{(t)} \right\}_{t=1}^T \triangleq [\mathbf{x}^{(1)\top} \quad \mathbf{x}^{(2)\top} \quad \dots \quad \mathbf{x}^{(T)\top}]^T, \quad (8)$$

which stacks a collection of tile-specific vectors into a single global vector.

Using this operator, the received snapshot at time  $n$  across all tiles can be compactly written as

$$\mathbf{y}[n] = \left\{ \mathbf{y}^{(t)}[n] \right\}_{t=1}^T \in \mathbb{C}^{TN}. \quad (9)$$

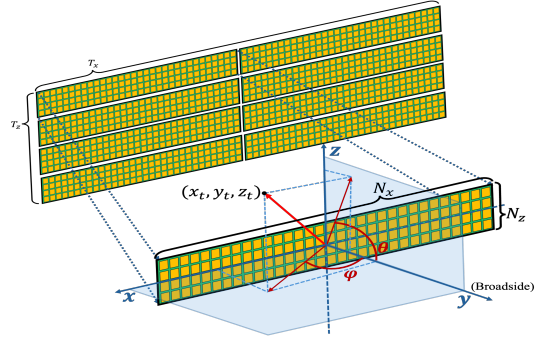


Fig. 1: Tiled UPA geometry illustrating the  $T_z \times T_x$  tile partitioning, the per-tile subarray structure with  $N_z \times N_x$  elements, and the definitions of elevation ( $\theta$ ) and azimuth ( $\varphi$ ) angles corresponding to the target location  $(x_t, y_t, z_t)$ .

### B. Conventional MVDR Beamforming

The objective of MVDR beamforming is to suppress interference and noise while preserving the signal arriving from a desired spatial direction.

The theoretical covariance matrix is defined as

$$\mathbf{R} = \mathbb{E} [\mathbf{y}[n] \mathbf{y}^H[n]], \quad (10)$$

and its empirical estimate based on  $n_t$  snapshots is

$$\hat{\mathbf{R}} = \frac{1}{n_t} \sum_{n=1}^{n_t} \mathbf{y}[n] \mathbf{y}^H[n]. \quad (11)$$

In each subband, for a given target index  $k$ , the MVDR correlator vector  $\mathbf{c}_k$  is computed by solving the following optimization problem:

$$\begin{aligned} \min_{\mathbf{c}_k} \quad & \mathbf{c}_k^H \hat{\mathbf{R}} \mathbf{c}_k \\ \text{subject to} \quad & \mathbf{c}_k^H \mathbf{a}_k = 1. \end{aligned} \quad (12)$$

where  $\mathbf{a}_k$  denotes the global steering vector of the  $k$ -th source, obtained by concatenating the per-tile steering vectors,

$$\mathbf{a}_k = \left\{ \mathbf{a}_k^{(t)} \right\}_{t=1}^T \in \mathbb{C}^{TN}. \quad (13)$$

The closed-form solution for the correlator vector is

$$\mathbf{c}_k = \frac{\hat{\mathbf{R}}^{-1} \mathbf{a}_k}{\mathbf{a}_k^H \hat{\mathbf{R}}^{-1} \mathbf{a}_k}. \quad (14)$$

Applying the correlator  $\mathbf{c}_k$  to the received vector  $\mathbf{y}[n]$  (i.e.  $\mathbf{c}_k^H \mathbf{y}[n]$ ) produces the beamformer output targeting the direction of  $k$ -th source.

## III. PROPOSED SYSTEM

### A. Overview

Figure 2 illustrates the processing flow of the proposed coordinated tiled windowed-beamspace MVDR architecture. After channelization, each tile operates independently on its  $N_z \times N_x$  subarray by applying a 2D spatial DFT to obtain a beamspace representation of the received snapshot. An AoA dependent window selects a fixed  $W_z \times W_x$  region of the

beamspace output, yielding a reduced-dimension  $W \times 1$  vector per tile.

The windowed outputs from all  $T$  tiles are then concatenated into a global  $TW \times 1$  beamspace snapshot, which serves as the input to a centralized MVDR processor. This coordinated design preserves the full-aperture spatial resolution while distributing the computationally intensive spatial transforms across tiles and performing covariance estimation and beamforming only in the reduced beamspace domain. The resulting MVDR outputs across all  $K$  targets are subsequently passed to the wideband synthesizer to produce the proper output for final range-Doppler processing.

This architecture enables scalable wideband operation by combining local dimension reduction at each tile with global coherent beamforming using a compact beamspace representation.

### B. Beamspace Transformation and Windowing

To enable scalable spatial processing in the tiled architecture, each tile projects its received signal into beamspace using a two-dimensional discrete Fourier transform. Let  $\mathbf{D}_N \in \mathbb{C}^{N \times N}$  denote the unitary  $N$ -point DFT matrix with entries

$$[\mathbf{D}_N]_{m,n} = \frac{1}{\sqrt{N}} e^{-j \frac{2\pi}{N} (m-1)(n-1)}, \quad m, n = 1, \dots, N.$$

The beamspace transform for a tile with  $N_z$  vertical and  $N_x$  horizontal antenna elements is given by the Kronecker product

$$\mathbf{D} = \mathbf{D}_{N_x}^\top \otimes \mathbf{D}_{N_z} \in \mathbb{C}^{N \times N}, \quad N = N_z N_x.$$

To reduce dimensionality, we apply an angle-of-arrival dependent beamspace window that extracts the spatial DFT bins associated with the  $k$ -th target. Let  $\mathbf{S}_{W_z}^{(k)} \in \mathbb{R}^{W_z \times N_z}$  and  $\mathbf{S}_{W_x}^{(k)} \in \mathbb{R}^{W_x \times N_x}$  denote the vertical and horizontal binary selector matrices that extract  $W_z$  and  $W_x$  beamspace components, respectively, centered around the DFT location corresponding to the  $k$ -th target's angle of arrival. This selects a total of  $W = W_z W_x$  beamspace coefficients from the original  $N = N_z N_x$  samples.

The full 2D windowing operator for the  $k$ -th target is constructed as

$$\mathbf{S}_k = \mathbf{S}_{W_x}^{(k)\top} \otimes \mathbf{S}_{W_z}^{(k)} \in \mathbb{R}^{W \times N}.$$

For tile  $t$ , the corresponding beamspace dimension-reduced snapshot of the  $k$ th target is

$$\tilde{\mathbf{y}}_k^{(t)}[n] = \mathbf{S}_k \mathbf{D} \mathbf{y}^{(t)}[n] \in \mathbb{C}^W. \quad (15)$$

Finally, the global windowed beamspace snapshot across all tiles is obtained using the concatenation operator defined in (8):

$$\tilde{\mathbf{y}}_k[n] = \left\{ \tilde{\mathbf{y}}_k^{(t)}[n] \right\}_{t=1}^T \in \mathbb{C}^{TW}. \quad (16)$$

### C. Reduced-Dimension MVDR

Given the dimension-reduced signal  $\tilde{\mathbf{y}}_k[n] \in \mathbb{C}^{TW}$ , we compute the beamspace MVDR weights using the same formulation as in Section II. Replacing  $\mathbf{y}[n]$  in Eq. 11 with  $\tilde{\mathbf{y}}_k[n]$  yields the windowed beamspace covariance matrix  $\tilde{\mathbf{R}}_k \in \mathbb{C}^{TW \times TW}$ , which captures the spatial structure of the reduced beamspace signal. Using this matrix in Eq. 14, we obtain the reduced-dimension MVDR correlator:

$$\tilde{\mathbf{c}}_k = \frac{\tilde{\mathbf{R}}_k^{-1} \tilde{\mathbf{a}}_k}{\tilde{\mathbf{a}}_k^H \tilde{\mathbf{R}}_k^{-1} \tilde{\mathbf{a}}_k} \in \mathbb{C}^{TW}, \quad (17)$$

where  $\tilde{\mathbf{a}}_k = \left\{ \mathbf{S}_k \mathbf{D} \mathbf{a}_k^{(t)} \right\}_{t=1}^T$  is the windowed beamspace steering vector corresponding to the target direction  $k$ .

To interpret the beamspace MVDR weights in the full antenna domain, we lift them back through the adjoint of the beamspace transform. Since the same beamspace transformation is applied to every tile, we first define the corresponding per-tile projection matrix

$$\mathbf{B}_k \triangleq \mathbf{S}_k \mathbf{D} \in \mathbb{C}^{W \times N}, \quad (18)$$

To apply this operator to the entire tiled array, we use a block-diagonal transformation expressed compactly through the Kronecker product with the identity matrix as

$$\tilde{\mathbf{y}}[n] = (\mathbf{I}_T \otimes \mathbf{B}_k) \mathbf{y}[n]. \quad (19)$$

Given the global beamspace MVDR weight vector  $\tilde{\mathbf{c}}_k \in \mathbb{C}^{TW}$ , the corresponding lifted antenna-space correlator is defined as

$$\hat{\mathbf{c}}_k \triangleq (\mathbf{I}_T \otimes \mathbf{B}_k^H) \tilde{\mathbf{c}}_k \in \mathbb{C}^{TN}, \quad (20)$$

The lifted weight vector enables direct comparison with full-dimensional antenna-space beamformers and reveals the corresponding beam pattern and correlator structure in the original array domain.

## IV. PERFORMANCE EVALUATION

### A. Dataset

We evaluate the proposed architecture using a simulated wideband radar dataset whose geometry, target ranges, and radial velocities are derived from the government-furnished data for the DARPA SOAP (Scalable On-Array Processing) program. The spatial layout of the scene and the angular distribution of the targets follow those of the original SOAP dataset, ensuring that the simulated environment depicted in Fig. 3 reflects realistic radar operations.

While the SOAP GFD models interferers using a variety of communication and radar signals, we use a simplified wideband jammer model for the interfering sources. Each interferer transmits spatially white Gaussian symbols with a specified power level relative to the targets, enabling controlled analysis of interference suppression under different interference-to-target power ratios.

The evaluation spans five scenarios, labeled A through E, with the number of interferers increasing from Scenario A

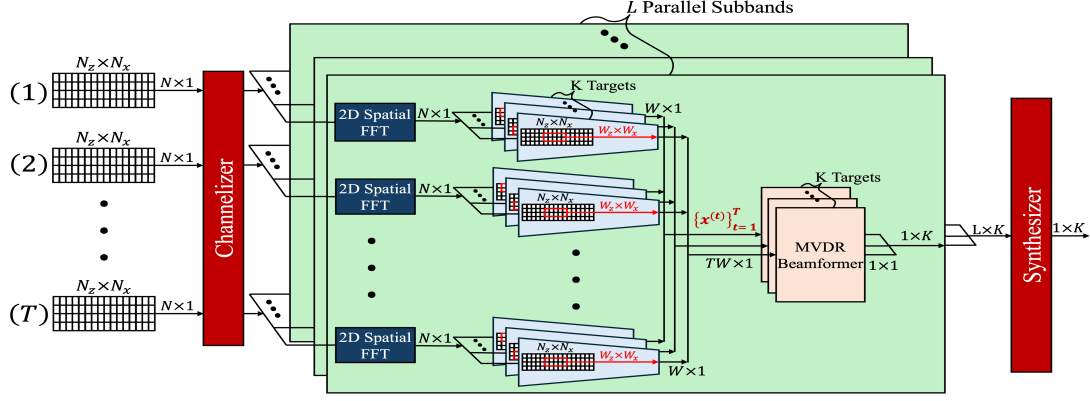


Fig. 2: Coordinated tiled beamspace MVDR processing for wideband radar signals. After channelization, each tile performs 2D spatial FFT projection and AoA-dependent beamspace windowing to produce  $W \times 1$  reduced-dimension vectors per target. The  $T$  tile outputs are concatenated into a global  $TW \times 1$  vector that feeds a centralized MVDR beamformer, followed by synthesis of a wideband signal for standard range-Doppler processing.

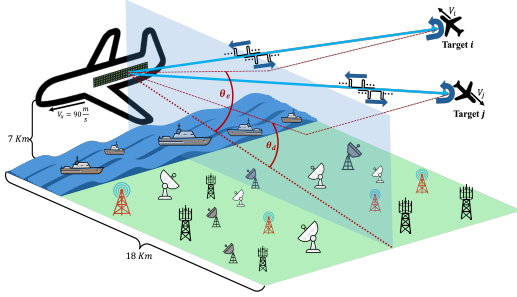


Fig. 3: Simulated environment with airborne targets with ground- and sea-based interferers. Targets  $i$  and  $j$  are in Easy and Difficult modes, respectively.

to Scenario E. Each scenario is provided in two geometric configurations: an *Easy mode* (index 1) in which targets exhibit greater elevation separation from the ground, and a *Difficult mode* (index 2) in which this separation is reduced, resulting in smaller elevation angles.

### B. Experimental Setup

We evaluate the proposed tiled windowed-beamspace MVDR architecture using the simulated wideband radar dataset described in Section IV-A. A full  $16 \times 64$  (1024 element) array is partitioned into a  $4 \times 2$  grid of tiles, where each tile contains a  $4 \times 32$  antenna subarray and performs local beamspace projection and AoA-dependent windowing as outlined in Section III-B. The wideband received signal is channelized into  $L = 32$  narrowband subbands using FFT-based channelization, and each subband is processed independently using the coordinated tiled MVDR framework.

To quantify the gains from coordinated tiling, we compare the proposed architecture against a single-array windowed beamspace MVDR implementation. Target detection is performed by applying a 1D CFAR processor across all velocity bins of the range-Doppler map, with a threshold set at

10 dB above the estimated noise floor. Detection accuracy is quantified in terms of range and velocity estimation error, and we examine how performance varies between the single-array and tiled coordinated implementations under identical interference conditions.

### C. Numerical Results

We compare the detection performance of the proposed coordinated tiled windowed-beamspace MVDR architecture against a single-array windowed beamspace MVDR implementation. Each method applies its own appropriately sized beamspace window, determined by the dimensions of the corresponding subarray or tile, as described in Section IV-B.

To highlight the performance gap under mild and severe interference conditions, we present results for two representative scenarios: A1 (least severe) and E2 (most severe). In Scenario A1, the coordinated tiled processor maintains reliable detection performance even when the interference power is increased to more than 120 dB above the target power, substantially exceeding the operating conditions of the original dataset. For Scenario E2, which reflects the harshest geometry and interference placement, both methods are evaluated under interference levels up to 80 dB above the target power, matching the strongest interference conditions observed in the original dataset and applied uniformly across all interferers in our simulations.

For each target, we compute a detection SINR defined as the ratio between the peak power at the target's range-velocity bin and the interference-plus-noise floor estimated via cell averaging in the surrounding CFAR stencil. This metric captures the quality of the detection output, including robustness against false alarms and the ability to reliably set a detection threshold, while also reflecting the underlying interference suppression performance of the beamformer.

Figures 4 and 5 show the range and velocity estimation errors for the single-array beamspace MVDR and the proposed coordinated tiled MVDR architecture. In both scenarios, each

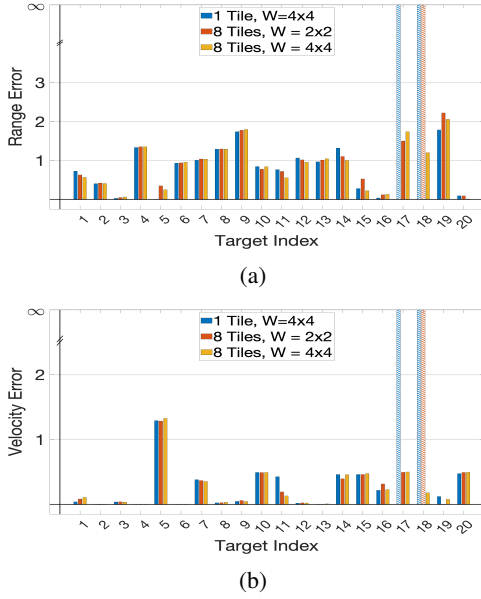


Fig. 4: Range and velocity estimation errors for Scenario A1.

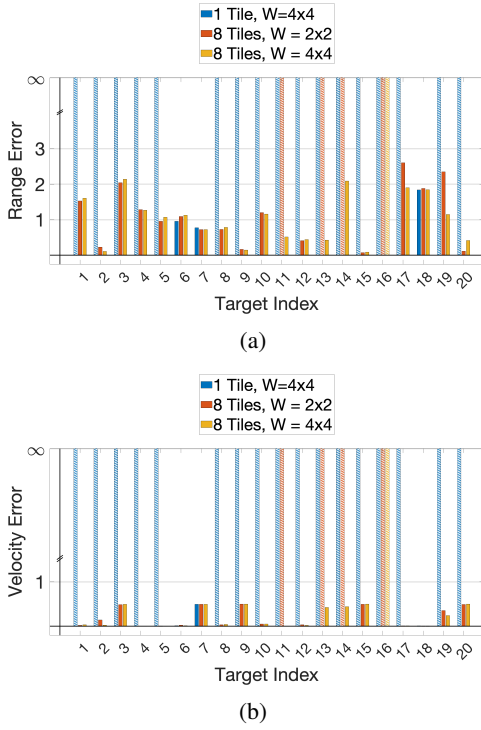


Fig. 5: Range and velocity estimation errors for Scenario E2.

tile operates with a beamspace window that is substantially smaller than its underlying antenna dimension. As a result, even if the per-tile window size is kept equal to the window size used in the single-array processor, the total beamspace dimension in the tiled architecture remains much smaller than that of full-dimensional MVDR. Coordinated processing across tiles further improves scalability: recovering full-

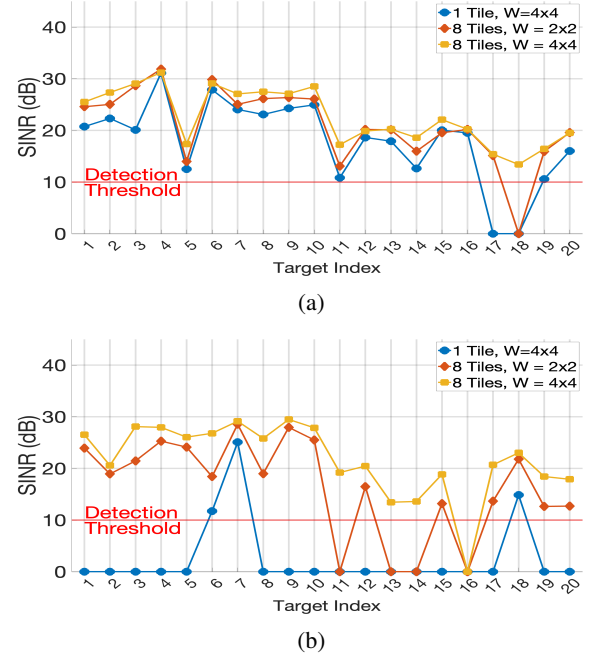


Fig. 6: SINR at the target grid points for both processing methods: (a) Scenario A1 and (b) Scenario E2.

aperture performance requires only a modest increase in per-tile window size, far smaller than the increase in total antenna count obtained by adding tiles. This demonstrates a key advantage of beamspace processing—its effective dimensionality grows slowly with array size due to energy concentration, allowing the tiled system to outperform the single-array processor with significantly fewer beamspace coefficients.

Across both A1 and E2 scenarios, the coordinated tiled MVDR detects more targets and exhibits lower range and velocity errors for detected targets. Missed targets are shown in the figures using hatched bars, and their corresponding errors are depicted symbolically as infinity to indicate detection failure.

The SINR results shown in Figure 6 further highlight the advantage of the coordinated tiled MVDR architecture. Across both scenarios, the coordinated approach achieves consistently higher SINR at the target detection bins compared to the single-array processor. Targets with SINR reported as zero correspond to missed detections, since no valid CFAR peak is present at the target's true range-velocity location.

The performance gap between the two methods becomes more pronounced in Scenario E2, where the interference environment is significantly more severe. In this case, the coordinated tiled processor maintains higher SINR for a larger fraction of the targets, demonstrating significantly increased robustness to strong interference than with a single tile.

Using the lifted correlators, we can also characterize the effective beamforming pattern for target  $k$  in the original antenna domain. For any azimuth-elevation pair  $(\varphi, \theta)$ , the



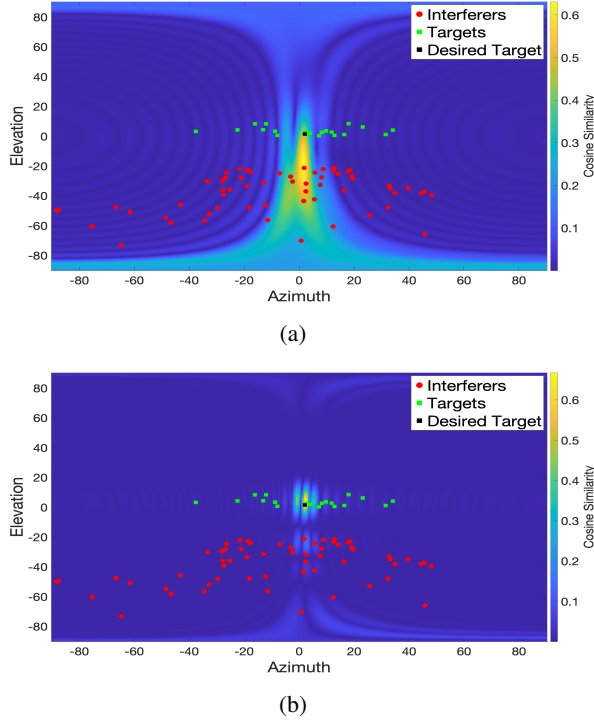


Fig. 7: Beamforming patterns for target 9 in  $E_2$  and in the center subband: (a) single-array beamspace processing with a  $4 \times 4$  window, and (b) coordinated tiled beamspace processing with a  $2 \times 2$  window per tile. The tiled architecture achieves a narrower mainlobe and deeper nulls despite a significantly reduced per-tile dimension.

normalized beam response is defined as

$$P_k(\varphi, \theta) = \frac{|\langle \hat{\mathbf{c}}_k, \mathbf{a}(\varphi, \theta) \rangle|}{\|\hat{\mathbf{c}}_k\|_2 \|\mathbf{a}(\varphi, \theta)\|_2}, \quad (21)$$

which corresponds to the cosine similarity between the lifted correlator and the steering vector at  $(\varphi, \theta)$ .

Figure 7 compares this beamforming pattern for a representative target under (a) single-tile processing with a  $4 \times 4$  beamspace window (i.e., a 16-dimensional observation) and (b) coordinated tiled processing with a  $2 \times 2$  per-tile beamspace window (i.e., resulting in a 32-dimensional observation when aggregated over 8 tiles). The tiled configuration produces a narrower mainlobe, deeper spatial nulls, and less noise enhancement, explaining its improved detection performance. Notably, even though the tiled array has eight times more elements than a single array, coordinated processing over 8 tiles requires only a doubling of the observation dimension to achieve a far superior beam pattern, illustrating the scalability of the proposed approach.

## V. CONCLUSION

This work presented a coordinated beamspace MVDR architecture for scalable wideband radar processing using tiled massive arrays. Computations are parallelized over tiles, exploiting energy concentration in beamspace within each tile, across subbands, and across targets: coordinated dimension-reduced

MVDR across tiles enables utilization of the full array aperture for each target. Numerical evaluations in challenging interference scenarios demonstrate that coordinated tile processing consistently yields lower range and velocity estimation errors and higher SINR, even when operating with reduced per-tile beamspace dimensions relative to a single tile. These results highlight a key advantage of beamspace domain techniques: the ability to scale to much larger apertures without incurring the prohibitive computational burden associated with full-dimensional antenna-space methods. Ongoing research focuses on methods for further reduction in computational complexity and inter-tile communication, and on hardware-signal processing co-design for implementing the proposed architectures.

## ACKNOWLEDGMENT

This work was supported in part by the Defense Advanced Research Projects Agency (DARPA) SOAP program, and in part by the Center for Ubiquitous Connectivity (CUBIC), sponsored by Semiconductor Research Corporation (SRC) and DARPA under the JUMP 2.0 program.

## REFERENCES

- [1] Y.-S. Yoon and M. G. Amin, "High-resolution through-the-wall radar imaging using beamspace music," *IEEE Transactions on Antennas and Propagation*, vol. 56, no. 6, pp. 1763–1774, 2008.
- [2] Y.-S. Yoon, M. G. Amin, and F. Ahmad, "Mvdr beamforming for through-the-wall radar imaging," *IEEE Transactions on Aerospace and Electronic Systems*, vol. 47, no. 1, pp. 347–366, 2011.
- [3] F. Nai, S. M. Torres, and R. D. Palmer, "Adaptive beamspace processing for phased-array weather radars," *IEEE Transactions on Geoscience and Remote Sensing*, vol. 54, no. 10, pp. 5688–5698, 2016.
- [4] Y. Jin and B. Friedlander, "Beamspace array processing for moving sources," in *Conference Record of the Thirty-Sixth Asilomar Conference on Signals, Systems and Computers, 2002.*, vol. 1. IEEE, 2002, pp. 871–875.
- [5] Q. Wang and H. You, "Mvdr beam-space pre-processing for wideband sources doa estimation," in *2008 Second International Symposium on Intelligent Information Technology Application*, vol. 2. IEEE, 2008, pp. 1091–1094.
- [6] Y. Doisy, L. Deruaz, and R. Been, "Interference suppression of subarray adaptive beamforming in presence of sensor dispersions," *IEEE Transactions on Signal Processing*, vol. 58, no. 8, pp. 4195–4212, 2010.
- [7] M. D. Zoltowski, G. M. Kautz, and S. D. Silverstein, "Simultaneous sector processing via root-music for large sensor arrays," in *Fifth ASSP Workshop on Spectrum Estimation and Modeling*. IEEE, 1990, pp. 372–376.
- [8] M. Abdelghany, U. Madhow, and A. Tölli, "Beamspace local lmmse: An efficient digital backend for mmwave massive mimo," in *2019 IEEE 20th International Workshop on Signal Processing Advances in Wireless Communications (SPAWC)*. IEEE, 2019, pp. 1–5.
- [9] M. Abdelghany, M. E. Rasekh, and U. Madhow, "Scalable nonlinear multiuser detection for mmwave massive mimo," in *2020 IEEE 21st International Workshop on Signal Processing Advances in Wireless Communications (SPAWC)*. IEEE, 2020, pp. 1–5.
- [10] C. Cebeci, O. D. Noroozi, and U. Madhow, "Scaling mmwave mu-mimo: Information-theoretic guidance using real-world data," in *2024 58th Asilomar Conference on Signals, Systems, and Computers*. IEEE, 2024, pp. 1620–1624.
- [11] O. D. Noroozi, J. Han, W. Tang, Z. Zhang, and U. Madhow, "Scaling wideband massive mimo radar via beamspace dimension reduction," in *2025 61st Allerton Conference on Communication, Control, and Computing Proceedings*. Allerton Conference on Communication, Control, and Computing, 2025.
- [12] J. Han, C. Cebeci, W. Tang, Z. Zhang, and U. Madhow, "Tiled beamspace processing for scaling mmwave massive mu-mimo," in *2024 IEEE 100th Vehicular Technology Conference (VTC2024-Fall)*. IEEE, 2024, pp. 1–6.